Superconductor Science and Technology

PAPER

# Persistence of the Nb(100) surface oxide reconstruction at elevated temperatures

To cite this article: Alison A McMillan *et al* 2020 *Supercond. Sci. Technol.* **33** 105012



IOP Publishing Superconductor Science and Technology
Supercond. Sci. Technol. **33** (2020) 105012 (7pp) https://doi.org/10.1088/1361-6668/abaec0

# Persistence of the Nb(100) surface oxide reconstruction at elevated temperatures

**Alison A McMillan, Jacob D Graham, Sarah A Willson, Rachael G Farber, Caleb J Thompson and S J Sibener**

The James Franck Institute and Department of Chemistry, The University of Chicago, 929 E. 57th Street, Chicago, IL 60637, United States of America

E-mail: s-sibener@uchicago.edu

Received 20 June 2020, revised 23 July 2020
Accepted for publication 12 August 2020
Published 10 September 2020

**Abstract**

Helium atom scattering and Auger electron spectroscopy (AES) are used to characterize the $(3 \times 1)$-O reconstruction of the Nb(100) surface at elevated temperatures. Persistent helium diffraction peaks and specular lineshape analysis indicate that the oxide structure persists, apparently unchanged, until surface temperatures of at least 1130 K. In a complementary experiment, AES oxygen to niobium ratios for Nb(100) show little to no change when the surface temperature is varied from 300 K to 1150 K. These data inform future development of superconducting radio frequency (SRF) cavities. In particular, these findings demonstrate the important role that persistent niobium oxides will play in the optimization of thin film growth strategies and coating procedures for $Nb_3Sn$ and other next–generation SRF superconducting alloy materials.

Keywords: niobium, niobium oxides, high temperature surface structure, helium atom diffraction, auger spectroscopy, superconducting radio frequency materials, $Nb_3Sn$

(Some figures may appear in colour only in the online journal)

## 1. Introduction

Niobium has become the material of choice for modern superconducting radio frequency (SRF) cavities in particle accelerators. Its low surface resistance ($R_S$), high critical temperature ($T_C$), and relatively high cavity quality ($Q$) factor at large fields all have contributed to its successful utilization in SRF cavities [1–4]. In addition, pure Nb is relatively soft and ductile, which allows it to be formed and welded into the cavity geometries required to optimize $Q$ factors and accelerating gradients [1]. Extensive research has been performed on these cavities and enables them to operate close to the fundamental limits of Nb [3–9]. Future progress, then, rests on the development of new materials: one of the most promising options is $Nb_3Sn$. Theoretical and experimental advances show that $Nb_3Sn$ cavities could yield higher $Q$ factors with larger accelerating gradients at higher operational temperatures than traditional Nb cavities [10–15], improving performance while also greatly reducing the cost of infrastructure and cryogens.

Unlike Nb, there are substantial issues associated with making cavities from $Nb_3Sn$ [3]. While its brittle nature and poor thermal conductivity prevent it from being fashioned into a cavity directly, thin $Nb_3Sn$ coatings formed on Nb have shown promising results [3, 16]. This process typically involves coating an existing Nb cavity with Sn, and then annealing at high temperatures to form the $Nb_3Sn$ thin film at or near the surface [6, 17]. Research into the microscopic formation of these thin films is necessary for advancement of SRF technology.

One complication present in the growth of $Nb_3Sn$ thin films is the role of Nb's native oxide layer. Nb is highly reactive to oxygen and its surface usually is covered by one of many possible oxide structures, both in air and in vacuum [18, 19]. The oxygen exposures required to reach these different oxide structures, as well as the structures themselves, have been well characterized [18–22]. Generally, a thick insulating $Nb_2O_5$ layer dominates the surface in air, while thin ordered $(n \times 1)$-O domains ('ladders') form readily on a Nb(100) surface after high temperature annealing in vacuum [20, 23–25].

 

As a refractory metal, Nb has a high melting temperature of 2741 K [26]. The oxygen in Nb starts to desorb as NbO and $NbO_2$ [27, 28] above 1900 K [18] in ultra-high vacuum (UHV), and it is not until Nb is heated above 2500 K that pure, clean, oxygen-free Nb is observed [18, 27–31]. The extreme temperatures needed to remove oxygen mean that the Nb SRF cavities are coated in an oxide layer, and that the Sn deposited to form $Nb_3Sn$ is deposited on one of many Nb oxides. The growth morphology of $Nb_3Sn$ on Nb is dependent on the interaction of Sn with the oxide layer. Thus, a complete, temperature–dependent, microscopic understanding of the Nb oxide surface is critical to the development of consistent, well-formed $Nb_3Sn$ thin films. Such understanding will allow for the development of alloy growth procedures with improved overall quality, homogeneity, and stoichiometry, enhancing critical operational SRF characteristics in high fields.

A key, missing factor in the literature is the nature of the Nb oxide surface at elevated temperatures. Up until now, studies have been limited to analyses at or below room temperature: thermal history and desorption temperatures are known, but the structure and stoichiometry at high temperatures has not been elaborated. In $Nb_3Sn$ SRF cavity fabrication processes, the Nb surface temperature is elevated during Sn nucleation, annealing, and degassing [3, 6, 17]. An understanding of the Nb oxide surface at elevated temperatures will guide current and new routes for improved $Nb_3Sn$ cavity production. To our knowledge, this combined helium atom scattering (HAS) and Auger electron spectroscopy (AES) study represents the first investigation of the Nb(100) oxide ladder structures at elevated temperatures, and it is one of the few *in-situ* studies of metal oxide structures at high temperatures.

HAS is a unique, nondestructive, surface sensitive technique that elucidates surface structure and dynamics [32]. The helium atoms are neutral probes that scatter off the electron cloud a few angstroms away from the surface: the surface is not damaged in any way [33–35]. HAS is particularly suited for examining surface structure at elevated temperatures. Unlike in typical low-energy electron diffraction (LEED), where electron bombardment heating presents experimental challenges, the neutral helium probe is not affected by the high voltages required for electron bombardment. Scanning tunneling microscopy (STM) also becomes very difficult at extremely high sample temperatures, due to atomic thermal fluctuations and instrument instability [36]. Debye–Waller attenuation of scattered He does become increasingly more important at elevated surface temperatures [33], but if the crystal is sufficiently reflective, diffracted He signal can be seen above the diffuse scattering background and the surface structure obtained.

## 2. Experimental

### 2.1. HAS—methods and sample preparation

The surface structure of Nb(100) was characterized with a UHV HAS apparatus that has high momentum and energy resolution. The apparatus has been described in detail elsewhere but is summarized here [37]. The HAS instrument consists of three regions: a differentially pumped beam source, a sample chamber, and a rotatable detector arm, resulting in a total helium flight path of 1.0701 m (chopper-to-crystal distance of 0.4996 m, crystal-to-ionizer distance of 0.5705 m).

The helium was expanded through a 15 $\mu$m nozzle that was cooled by a closed-cycle helium refrigerator. This generated a nearly monoenergetic ($\Delta v/v \leq 1\%$), supersonic helium beam that was collimated into an approximately 4 mm spot on the crystal surface. A mechanical chopper modulated the beam prior to collision with the surface; a 50% duty cycle was used for angular distributions and a 1% duty cycle for time-of-flight measurements to determine the beam energy. The Nb(100) crystal was mounted on a six-axis manipulator that precisely controlled the incident angle, $\theta_i$, the azimuthal angle, $\phi$, and the tilt, $\chi$, with respect to the scattering plane. Sample temperatures ranging from 300 K to 1900 K were achieved using electron bombardment in combination with a closed-cycle helium refrigerator. Reflected helium atoms entered a triply differentially pumped, computer–controlled, rotatable detector arm; were ionized via electron bombardment; filtered using a quadruple mass spectrometer; and detected with an electron multiplier followed by pulse counting electronics. Angular distributions were obtained by rotating the detector at 0.2° increments while holding the incident angle and energy fixed. The overall instrument resolution was 0.45°. The incident helium beam was held at 21 meV ($k_i = 6.3$ Å$^{-1}$ and $T_n = 96.9$ K) so that the specular, first-order primitive, and $(3 \times 1)$-O superlattice diffraction peaks could be observed in the same angular distribution.

Nb(100) was obtained from the Surface Preparation Laboratory (Netherlands, 99.99% purity, ∼0.1° cut accuracy) and prepared in the HAS apparatus by cycles of annealing at and flashing to 1900 K. The primary initial impurities identified by AES were carbon, boron, sulfur, and nitrogen. Sputtering with 500 eV $Ne^+$ ions (3 $\mu$A maximum) removed the boron and sulfur contaminants while the combination of annealing and flashing eventually removed the carbon. Annealing and sputtering continued until AES analysis showed only niobium and oxygen present on the surface. Flashes to 1300 K were performed before experiments to remove any trace adsorbates from the crystal surface.

### 2.2. AES—methods and sample preparation

AES measurements of Nb(100) from the Surface Preparation Laboratory (Netherlands, 99.99% purity, ∼0.1° cut accuracy) were performed in a UHV experimental system composed of a STM chamber (UHV VT–STM, RHK Technology) and a preparation chamber equipped with AES capabilities, as previously described [23]. The Nb(100) crystal was cleaned via repeated cycles of $Ar^+$ ion sputtering and electron bombardment annealing at a sample temperature ($T_S$) of approximately 2100 K, as measured using a Mikron Infrared (MG–140) pyrometer. Surface cleanliness was confirmed by AES and STM

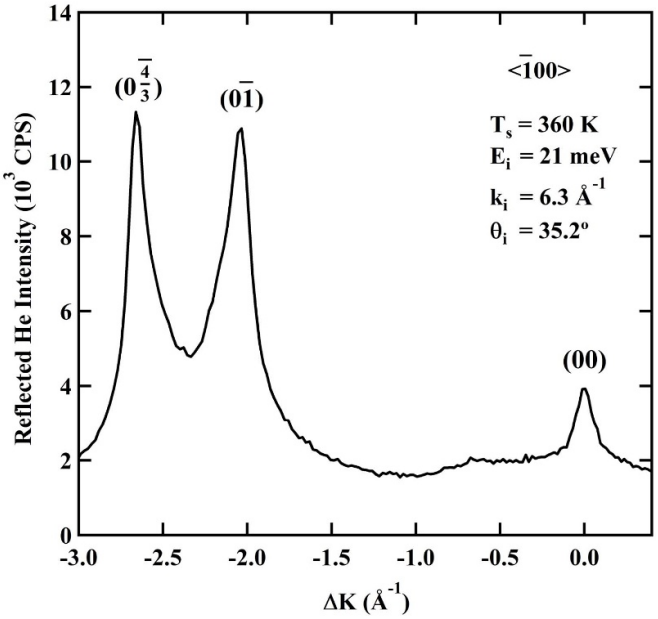


**Figure 1.** Representative diffraction spectrum for He on (3 × 1)-O/Nb(100) along the <$\bar{1}$00> symmetry axis as a function of parallel momentum exchange.

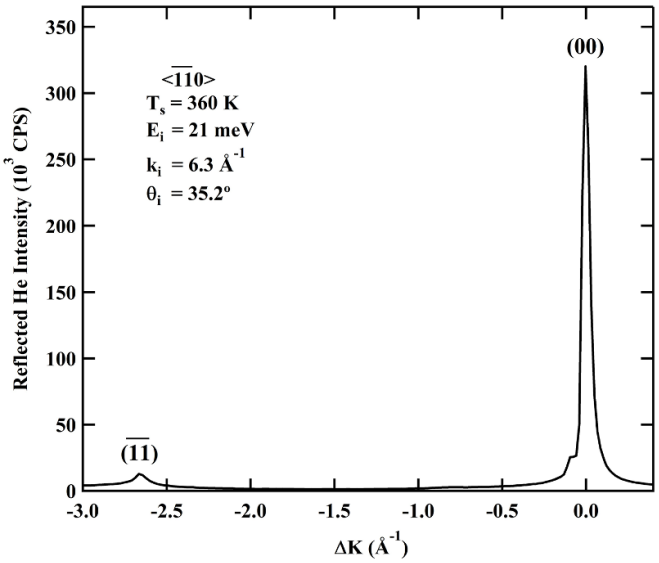


**Figure 2.** Representative diffraction spectrum for He on (3 × 1)-O/Nb(100) along the <$\bar{1}\bar{1}$0> symmetry axis as a function of parallel momentum exchange.

analyses, which showed the characteristic (3 × 1)-O superlattice with no surface contaminants [20, 23, 38].

## 3. Results and discussion

### 3.1. Helium diffraction

After preparation in vacuum, the Nb(100) surface reconstructs into a (3 × 1)-O ladder structure, as observed elsewhere [23]. Figure 1 shows an angular distribution of helium back-scattered from the Nb(100)/(3 × 1)-O surface along the <$\bar{1}$00>, ($\bar{\Gamma} - \bar{X}$) azimuthal direction. The diffraction spectrum was taken at a surface temperature of 360 K with an incident angle of $\theta_i = 35.2°$. The reproducibility of the surface was confirmed through repeated scans at $T_S = 360$ K after flashing the crystal to 1300 K. Three diffraction peaks are resolved clearly: a zeroth-order specular peak ($\theta_i = \theta_f$) at $\Delta K = 0$ Å$^{-1}$, a first-order, $(0\bar{1})$ diffraction peak at $\Delta K = -2.0$ Å$^{-1}$ ($\theta_f = 14.7°$), and a (3 × 1)-O superlattice, $\left(0\frac{\bar{4}}{3}\right)$ diffraction peak at $\Delta K = -2.6$ Å$^{-1}$ ($\theta_f = 9.1°$). These elastic diffraction peaks arise when the requirements for Bragg diffraction are satisfied, such that

$$\Delta K = k_i(\sin\theta_i - \sin\theta_f) = G_{mn} \tag{1}$$

where $\Delta K$ is the change in the surface-parallel component of the helium wavevector $k_i$; $\theta_i$ and $\theta_f$, respectively, are the initial and final scattering angles relative to the surface normal; and $G_{mn}$ is a linear combination of surface reciprocal lattice vectors. From the first-order, $(0\bar{1})$ diffraction peak, the Nb–Nb lattice spacing was determined to be 3.08 ± 0.02 Å, which corresponds favorably to surface lattice constants found through LEED measurements [20]. The diffraction peak at $\Delta K = -2.6$ Å$^{-1}$ was identified as (3 × 1)-O superlattice peak, since its $\Delta K$ value is approximately $\frac{4}{3}$ times that of the $(0\bar{1})$, primitive peak. This also aligns with previous LEED studies that show the (3 × 1)-O superlattice structure [20]. The intensities of both the $(0\bar{1})$ and $\left(0\frac{\bar{4}}{3}\right)$ peaks are far greater than that of the specular peak, which is in contrast to HAS from the bare Nb(100) surface and suggests an increase in surface corrugation as a result of the ladder structure [31, 39].

The angular distribution of the <$\bar{1}\bar{1}$0>, ($\bar{\Gamma} - \bar{M}$) azimuthal direction was determined and is shown in figure 2 at $T_S = 360$ K. In this direction, the specular peak is far more intense than in the <$\bar{1}$00> direction, again indicating a high surface corrugation. The small, secondary specular peak can be attributed to surface faceting from the anneal process and was ignored in analysis [31]. The peak at $\Delta K = -2.7$ Å$^{-1}$ corresponds to the $(\bar{1}\bar{1})$ diffraction peak.

The high intensity of the specular peak in the <$\bar{1}\bar{1}$0> direction allowed us to analyze the peak lineshape with minimal contributions from the diffuse elastic and multiphonon background seen in the <$\bar{1}$00> direction. The helium beam strikes the surface with a 4 mm spot size, averaging over many atomically flat terraces. The average width of these terraces has been shown to be approximately equal to the coherence length, $l_c$ [40, 41]. The specular peak broadening from the average domain size, $\Delta\theta_w$, can be found through a deconvolution of the measured specular peak full width half maximum (FWHM), $\Delta\theta_{exp}$, and the instrument function broadening, $\Delta\theta_{inst}$:

$$\Delta\theta_w^2 = \Delta\theta_{exp}^2 - \Delta\theta_{inst}^2. \tag{2}$$

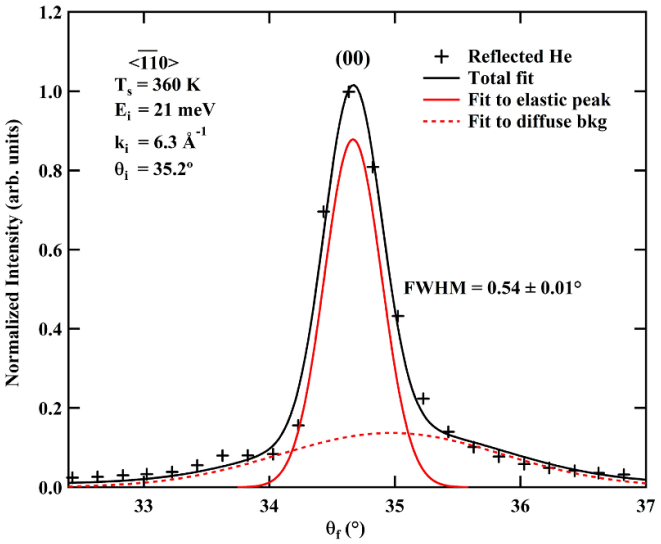


**Figure 3.** Width analysis of a specular ($\theta_i = \theta_f$) He diffraction peak on (3 × 1)-O/Nb(100) along the <$\bar{1}\bar{1}$0> symmetry axis, plotted vs. final scattered angle ($\theta_f$). The solid red line is a Gaussian fit to the coherent elastic peak, the dashed red line is a Gaussian fit to the diffuse elastic and multiphonon background, and the solid black line is the overall fit to the data (black crosses). The narrow, coherent elastic peak (solid red line) has a FWHM of 0.54 ± 0.01°.

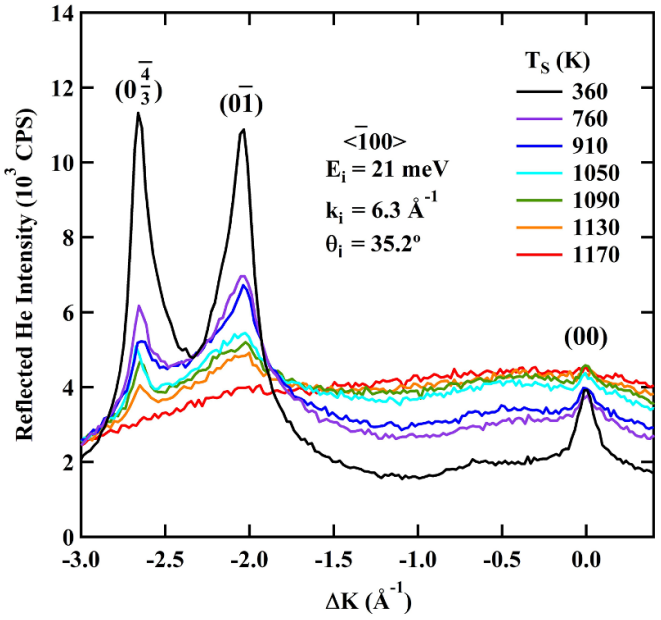


**Figure 4.** Decay of diffraction spectra for He on (3 × 1)-O/Nb(100) along the <$\bar{1}$00> symmetry axis as a function of surface temperature, plotted vs. parallel momentum exchange.

The coherence length then can be determined through the equation [41],

$$l_c = \frac{5.54}{\Delta\theta_w k_i \cos(\theta_f)}. \quad (3)$$

Figure 3 shows the fitting function used to determine the width of the specular peak. The normalized peak was fit with one sharp Gaussian function for the coherent elastic signal and one broad Gaussian for the diffuse elastic and multiphonon background signal [42]. With an overall instrument resolution of 0.45° and a measured specular FWHM of 0.54 ± 0.01°, the average domain size was found to be 210 ± 10 Å.

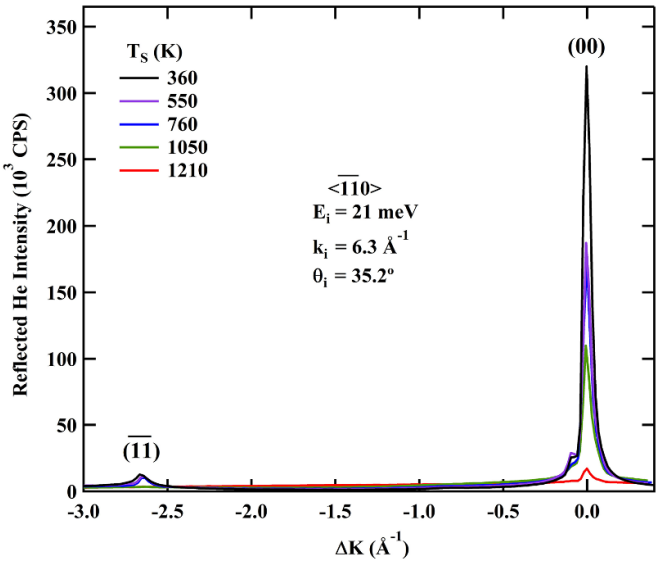


**Figure 5.** Decay of diffraction spectra for He on (3 × 1)-O/Nb(100) along the <$\bar{1}\bar{1}$0> symmetry axis as a function of surface temperature, plotted vs. parallel momentum exchange.

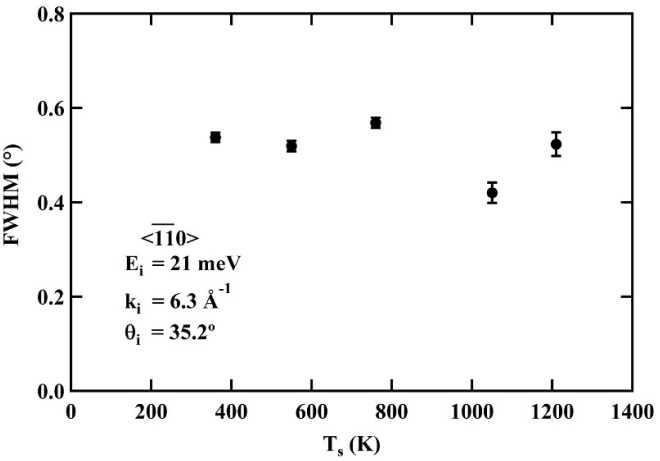


**Figure 6.** FWHM of Gaussian fits to the coherent elastic portion of specular ($\theta_i = \theta_f$) He diffraction peaks on (3 × 1)-O/Nb(100) along the <$\bar{1}\bar{1}$0> symmetry axis, plotted vs. surface temperature. All peaks were fit with two Gaussians, as illustrated in figure 3.

Diffraction spectra in the <$\bar{1}$00> direction, as a function of increasing temperature, are shown in figure 4. Surface stability at each temperature was determined by immediately repeating each scan; the identical scans indicated that the surface structure was unchanging. While the specular peak is enveloped by the background at around 1053 K, the $(0\bar{1})$ and $\left(0\frac{\bar{4}}{3}\right)$ diffraction peaks are visible up to at least 1130 K. At 1170 K, the peak intensities are lower than the detected background.

Temperature dependent spectra in the <$\bar{1}\bar{1}$0> direction are shown in figure 5. Spectra were recorded as a function

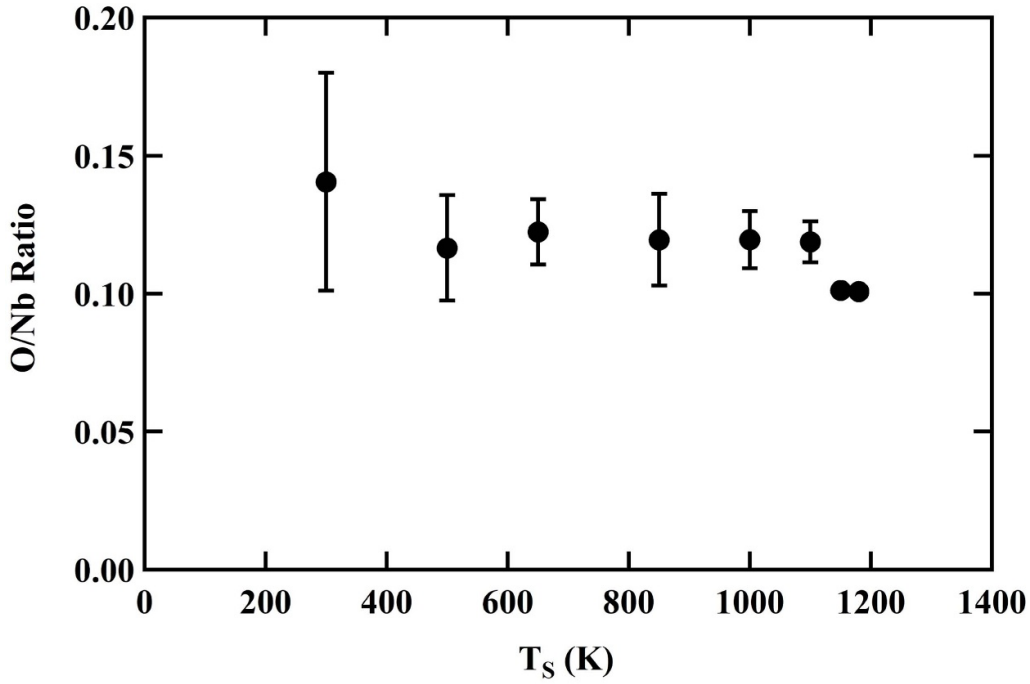


**Figure 7.** O/Nb AES ratios taken at $T_s$ between 300 K and 1150 K. There is no significant decrease in O content on Nb(100) below 1200 K.

of increasing temperature, except for the spectrum taken at 550 K, which was taken after a 1900 K flash. The specular intensities at five different surface temperatures were fit in a similar manner to that shown in figure 3, and the FWHM of each coherent elastic peak is shown in figure 6. HAS lineshapes are very sensitive to surface disorder [33, 39]; any oxygen dissolution or disorder caused by the elevated temperatures would dramatically increase the width of the specular peak. Instead, the width stays nearly constant as a function of surface temperature up to 1210 K, as seen in figure 6. This, in addition to the existence of the superlattice diffraction peak in figure 4 at 1130 K, indicate that the (3 × 1)-O superlattice remains unchanged on the Nb(100) surface up to at least 1130 K, and presumably up to at least 1210 K.

### 3.2. AES

A second Nb(100) single crystal was prepared in a separate UHV experimental system, which resulted in the (3 × 1)-O superlattice structure [23, 43]. In order to determine the concentration of surface oxygen on Nb(100) at elevated temperatures, a ratio of the peak-to-peak intensities of the principle O and Nb peaks were obtained, at 519 eV and 169 eV, respectively [44], for $T_S$ ranging from 300 K to 1150 K. The O/Nb ratios displayed in figure 7, plotted as a function of $T_S$, quantitatively describe the surface composition at elevated surface temperatures; the displayed error bars account for varying near-surface and surface oxide contributions.

Across the entire temperature range studied in this work, the O/Nb ratio is stable, providing evidence for a constant surface oxygen concentration up to 1150 K. The near surface does not lose oxygen from the thermal annealing [23], even though the subsurface oxygen content may vary due to the cleaning procedure and the amount of oxygen in the bulk, as seen by slight fluctuations in the O/Nb ratio at $T_S = 300$ K. The average measured Auger peak intensities did not change as a function of primary beam exposure time, indicating that the AES experiments did not modify the surface elemental composition over the course of data collection. Furthermore, the Nb(100) surface was analyzed by *in-situ*, room temperature STM following the AES measurements. The STM work confirmed that the surface remained covered by the characteristic (3 × 1)-O superlattice and that the sample was not damaged by the high temperature AES measurements. Residual gas analyzer spectra indicated that the oxide did not desorb within the studied temperature range, so any observed reduction in the O/Nb ratio denotes oxygen dissolution into the bulk crystal. However, based on the AES O/Nb ratios detailed in figure 7, there is no evidence of appreciable oxygen dissolution below 1200 K. This AES analysis confirms the HAS measurements that show no appreciable oxygen dissolution or disorder within the $T_S$ range studied.

## 4. Conclusion

HAS and AES provide evidence for the continued existence of a (3 × 1)-O ladder structure on the Nb(100) surface until at least 1130 K and, to our knowledge, this work is the first investigation of the niobium oxide surface at elevated temperatures. Helium diffraction peaks from the oxide structure were persistent until 1130 K, and the specular peak lineshapes indicated little to no surface disorder up to 1210 K. The constant AES oxygen to niobium peak ratios of Nb(100) also indicated that oxygen did not leave the surface either through dissolution or evaporation until above 1200 K, consistent with

previous studies [18, 20]. The unvaried oxide reconstruction at the investigated high temperatures informs future SRF cavity research and development. The next-generation method of coating Nb cavities with a thin film of $Nb_3Sn$ involves an initial nucleation step where the surface is held at about 770 K [3], below the 1130 K temperature measured here. Our research shows that Sn is nucleating on an oxide, not on bare Nb. This further illuminates the role of oxygen in the Sn deposition and cavity optimization processes. The oxide structure above 1130 K, including at approximately 1375 K [3] where the Sn-coated cavities are annealed, is still unknown, and would bring similarly interesting information to the discussion on SRF cavity production. Additional unanswered questions include Sn mobility, long-term stability, the mechanisms and kinetics for Sn incorporation into the Nb substrate, and the development $Nb_3Sn$ alloy materials with lower defect concentrations and higher chemical and spatial uniformity. These questions need to be addressed to realize the SRF community's ambitious goal to successfully implement this promising alloy in next-generation accelerator applications.

## Acknowledgments

S J S would like to acknowledge support from the US National Science Foundation under Award PHY-1549132, the Center for Bright Beams, and from the Air Force Office of Scientific Research Grant No. FA9550-19-1-0324. Preliminary work was partially supported by the US National Science Foundation under Award PHY-1535639. Support from the NSF-Materials Research Science and Engineering Center at The University of Chicago, Grant No. NSF-DMR-14-20709, also is gratefully acknowledged.

## ORCID iDs

Jacob D Graham https://orcid.org/0000-0002-9815-810X
Sarah A Willson https://orcid.org/0000-0001-7762-2746
Rachael G Farber https://orcid.org/0000-0002-9055-137X
S J Sibener https://orcid.org/0000-0002-5298-5484

## References

[1] Padamsee H 2001 The science and technology of superconducting cavities for accelerators *Supercond. Sci. Technol.* **14** R28–51
[2] Reece C E 2016 Continuous wave superconducting radio frequency electron linac for nuclear physics research *Phys. Rev. Accel. Beams* **19** 124801
[3] Posen S and Hall D L 2017 $Nb_3Sn$ superconducting radiofrequency cavities: fabrication, results, properties, and prospects *Supercond. Sci. Technol.* **30** 033004
[4] Ford D C, Cooley L D and Seidman D N 2013 Suppression of hydride precipitates in niobium superconducting radio-frequency cavities *Supercond. Sci. Technol.* **26** 105003
[5] Ma Q, Ryan P, Freeland J W and Rosenberg R A 2004 Thermal effect on the oxides on Nb(100) studied by synchrotron-radiation x-ray photoelectron spectroscopy *J. Appl. Phys.* **96** 7675–80
[6] Posen S and Liepe M 2014 Advances in development of $Nb_3Sn$ superconducting radio-frequency cavities *Phys. Rev. Spec. Top. Accel. Beams* **17** 112001
[7] Romanenko A, Grassellino A, Barkov F and Ozelis J P 2013 Effect of mild baking on superconducting niobium cavities investigated by sequential nanoremoval *Phys. Rev. Spec. Top. Accel. Beams* **16** 012001
[8] Grassellino A, Romanenko A, Sergatskov D, Melnychuk O, Trenikhina Y, Crawford A, Rowe A, Wong M, Khabiboulline T and Barkov F 2013 Nitrogen and argon doping of niobium for superconducting radio frequency cavities: a pathway to highly efficient accelerating structures *Supercond. Sci. Technol.* **26** 102001
[9] Grassellino A *et al* 2017 Unprecedented quality factors at accelerating gradients up to 45 $MVm^{-1}$ in niobium superconducting resonators via low temperature nitrogen infusion *Supercond. Sci. Technol.* **30** 094004
[10] Lee J, Mao Z, He K, Sung Z H, Spina T, Baik S-I, Hall D L, Liepe M, Seidman D N and Posen S 2020 Grain-boundary structure and segregation in $Nb_3Sn$ coatings on Nb for high-performance superconducting radiofrequency cavity applications *Acta Mater.* **188** 155–65
[11] Becker C, Posen S, Groll N, Cook R, Schlepütz C M, Hall D L, Liepe M, Pellin M, Zasadzinski J and Proslier T 2015 Analysis of $Nb_3Sn$ surface layers for superconducting radio frequency cavity applications *Appl. Phys. Lett.* **106** 082602
[12] Trenikhina Y, Posen S, Romanenko A, Sardela M, Zuo J-M, Hall D L and Liepe M 2018 Performance-defining properties of $Nb_3Sn$ coating in SRF cavities *Supercond. Sci. Technol.* **31** 015004
[13] Dickey J M, Strongin M and Kammerer O F 1971 Studies of thin films of $Nb_3Sn$ on Nb *J. Phys. D: Appl. Phys.* **42** 5808–20
[14] Porter R D, Arias T, Cueva P, Hall D L, Liepe M, Maniscalco J T, Muller D A and Sitaraman N 2018 Next generation $Nb_3Sn$ SRF cavities for linear accelerators *29th Linear Accelerator Conf.* pp 462–5
[15] Kneisel P, Stoltz O and Halbritter J 1979 Measurements of superconducting $Nb_3Sn$ cavities in the GHz range *IEEE Trans. Magn.* **15** 21–24
[16] Arnolds G and Proch D 1977 Measurement on a $Nb_3Sn$ structure for linear accelerator application *IEEE Trans. Magn.* **13** 500–3
[17] Posen S and Liepe M 2011 Stoichiometric $Nb_3Sn$ in first samples coated at Cornell *15th Conf. RF Supercondivity* pp 886–9
[18] Farrell H H, Isaacs H S and Strongin M 1973 The interaction of oxygen and nitrogen with the niobium (100) surface: II. Reaction kinetics *Surf. Sci.* **38** 31–52
[19] Farrell H H and Strongin M 1973 The interaction of oxygen and nitrogen with the niobium (100) surface: I. Morphology *Surf. Sci.* **38** 18–30
[20] An B, Fukuyama S, Yokogawa K and Yoshimura M 2003 Surface structures of clean and oxidized Nb(100) by LEED, AES, and STM *Phys. Rev.* B **68** 115423
[21] Lindau I and Spicer W E 1974 Oxidation of Nb as studied by the uv-photoemission technique *J. Phys. D: Appl. Phys.* **45** 3720–5
[22] Wang Y, Wei X, Tian Z, Cao Y, Zhai R, Ushikubo T, Sato K and Zhuang S 1997 An AES, UPS and HREELS study of the oxidation and reaction of Nb(110) *Surf. Sci.* **372** L285–90
[23] Veit R D, Kautz N A, Farber R G and Sibener S J 2019 Oxygen dissolution and surface oxide reconstructions on Nb(100) *Surf. Sci.* **688** 63–68
[24] Uehara Y, Fujita T, Iwami M and Ushioda S 2001 Single NbO nano-crystal formation on low temperature annealed Nb(001) surface *Surf. Sci.* **472** 59–62

[25] Arfaoui I, Cousty J and Guillot C 2004 A model of the $NbO_{x\approx1}$ nanocrystals tiling a Nb(110) surface annealed in UHV *Surf. Sci.* **557** 119–28
[26] Musket R G, McLean W, Colmenares C A, Makowiecki D M and Siekhaus W J 1982 Preparation of atomically clean surfaces of selected elements: a review *Appl. Surf. Sci.* **10** 143–207
[27] Franchy R, Bartke T U and Gassmann P 1996 The interaction of oxygen with Nb(110) at 300, 80 and 20 K *Surf. Sci.* **366** 60–70
[28] Pantel R, Bujor M and Bardolle J 1977 Continuous measurement of surface potential variations during oxygen adsorption on the (100), (110) and (111) faces of niobium using mirror electron microscope *Surf. Sci.* **62** 589–609
[29] Dawson P H and Tam W-C 1979 The interaction of oxygen with polycrystalline niobium studied using AES and low-energy SIMS *Surf. Sci.* **81** 464–78
[30] Usami S, Tominaga N and Nakajima T 1976 AES-LEED study of adsorption of common gases on the (100) planes W and Nb *Vacuum* **27** 11–16
[31] Hulpke E, Hüppauff M, Smilgies D-M, Kulkarni A D and de Wette F W 1992 Lattice dynamics of the niobium (001) surface *Phys. Rev.* B **45** 1820–8
[32] Hulpke E 1992 Introduction *Helium Atom Scattering from Surfaces* Springer Series in Surface Science vol 27 ed E Hulpke (Berlin: Springer) pp 1–4
[33] Farías D and Rieder K-H 1998 Atomic beam diffraction from solid surfaces *Rep. Prog. Phys.* **61** 1575–664
[34] Scoles G 1988 *Atomic and Molecular Beam Methods* vol 1 (Oxford: Oxford University Press)
[35] Scoles G 1992 *Atomic and Molecular Beam Methods* vol 2 (Oxford: Oxford University Press)
[36] Meyer E, Hug H J and Bennewitz R 2004 *Scanning Probe Microscopy: The Lab on a Tip* (Berlin: Springer)
[37] Gans B, Knipp P A, Koleske D D and Sibener S J 1992 Surface dynamics of ordered $Cu_3Au(001)$ studied by elastic and inelastic helium atom scattering *Surf. Sci.* **264** 81–94
[38] Li Y, An B, Xu X, Fukuyama S, Yokogawa K and Yoshimura M 2001 Surface structure of niobium-dioxide overlayer on niobium(100) identified by scanning tunneling microscopy *J. Appl. Phys.* **89** 4772–6
[39] Engel T and Rieder K-H 1982 Structural studies of surfaces with atomic and molecular beam diffraction *Structural Studies of Surfaces* Springer Tracts in Modern Physics vol 91 (Berlin: Springer) pp 55–180
[40] Comsa G 1979 Coherence length and/or transfer width? *Surf. Sci.* **81** 57–68
[41] Lapujoulade J, Lejay Y and Armand G 1980 The thermal attentuation of coherent elastic scattering of noble gas from metal surfaces *Surf. Sci.* **95** 107–30
[42] Becker J S, Brown R D, Johansson E, Lewis N S and Sibener S J 2010 Helium atom diffraction measurements of the surface structure and vibrational dynamics of $CH_3$-Si(111) and $CD_3$-Si(111) surfaces *J. Chem. Phys.* **133** 104705
[43] Veit R D, Farber R G, Sitaraman N S, Arias T A and Sibener S J 2020 Suppression of nano-hydride growth on Nb(100) due to nitrogen doping *J. Chem. Phys.* **152** 214703
[44] Davis L 1976 *Handbook of Auger Electron Spectroscopy* (Eden Prairie, MN: Physical Electronics Industries)